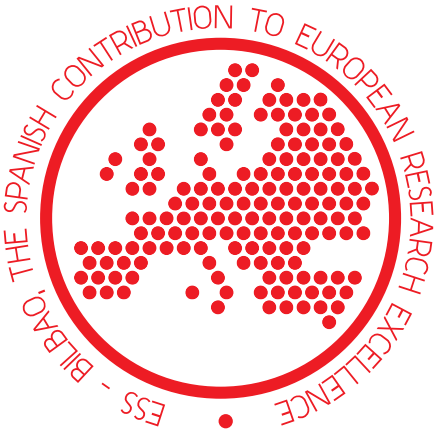

Target, Shaft and Rotating seal CFD analysis

Reference:	ESS-0066301
Date:	September 16, 2016
Revision:	0

Author	Review	Aprobed
J. Aguilar A. Aguilar M. Magan I. Herranz F. Sordo T. Mora R. Vivanco G. Bakedano L. Mena M. Mancisidor	F. Sordo	J. L. Martinez

Contents

1 Introduction

Neutron Spallation sources are devices designed to produce neutrons from spallation nuclear reactions. In order to produce this kind of reactions it is necessary to accelerate protons (H+ particles) using electromagnetic fields up to they get a huge amount of kinetic energy or speed close to light velocity. In that moment, protons are led to impact on a nucleus of a heavy atom (generally mercury, lead or tungsten) producing what it is known as spallation reaction.

The place where the reaction is produced it is known as Spallation Target and it is considered the neutron source. This Targets are complex devices, from an engineering point of view, where a huge amount of heat is deposited on the spallation material. In some cases, it is note that the heat density in the spallation target can be higher than fuel bars inside a nuclear power reactor, as a consequence the design of Spallation Target is a real engineering challenge. The ESS target is one of these cases.

The European Spallation Source (ESS) is an ambitious European project with a budget higher to 1800 M€. The aim of the project is to design, build and operate the most important and the bright spallation neutron source in the world. The ESS will use a proton beam with final power deposited on the target of 5 MW (five times higher than SNS and JPARC), which will impact on a tungsten Target cooled by helium gas.

The Target will be designed with a set of tungsten blocks placed inside of a wheel of 2.5-2.6 meter of diameter. Protons will impact at high speed on the wheel in a radial direction. Inside the wheel, helium flows at high velocity, cooling the tungsten blocks dissipating the heat produced by the nuclear reactions. The wheel rotates at a speed of 0.2-0.5 Hz, so the proton beam impacts on a different region of the wheel at a repetition rate of 14Hz, distributing the heat over the whole perimeter of the wheel.

The following sections describes the final optimization process for the flow pattern in the central region of the wheel and the shaft that minimizes the pressure drop of the system. Finally the complete analysis of the Target wheel and shaft is shown.

2 ESS Target configuration

The configuration of a 5 MW Spallation target is a complex process and there is no unique solution. Also it should be remarked that most of the activated material produced in spallation reactions will be confined inside the target. For that reason the target design is close related to ESS safety issues. In order to guide the selection of the target concept, ESS organized a working group so as to explore several Target options (Target Selection Concept Phase, TSCP). This working group explored several target options from 2010 to 2012[1].

After this process, ESS selected as final solution a solid rotating target cooled by helium. This solution was developed further by ESS and KIT along 2012-2013 and its final concept is

summarized on the TDR proposal.

On November 2014, ESS-Bilbao was choose as in-kind partner for Target Wheel, shaft and drive unit. The redesign works started on January 2015. Along this period, ESS-Bilbao has follow and optimization process summarized on the Report [2] that arrives to a new base line proposal in June 2015. The previous configurations analysis is not in the scope of this document.

The proposed new target configuration is based on 10x30x80 mm^3 tungsten bricks. These tungsten bricks are placed on an steel support (the "cassette"), in a cross flow configuration as it is shown on Figure 1. The coolant will move in the gap in between bricks removing the heat deposited by the proton beam. Taking into account the rotation of the wheel and the proton beam frequency, the accelerator shuts on each cassette with a frequency of 14/36 Hz.

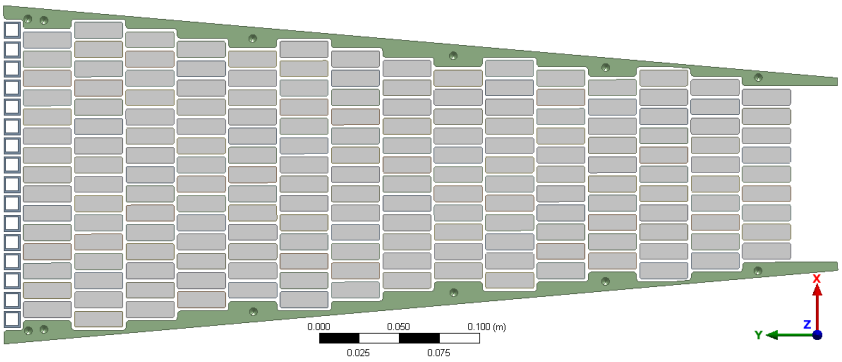

Figure 1: Tungsten bricks(grey) and turbulence generators final (blue) configuration on a Target Wheel sector.

The cassette withstand tungsten bricks and configures the inlet helium channels in the gap between ribs and target vessel (Figure 3). Finally, 36 of these cassettes will be assembled in a sectored wheel as it is shown on Figure 2.

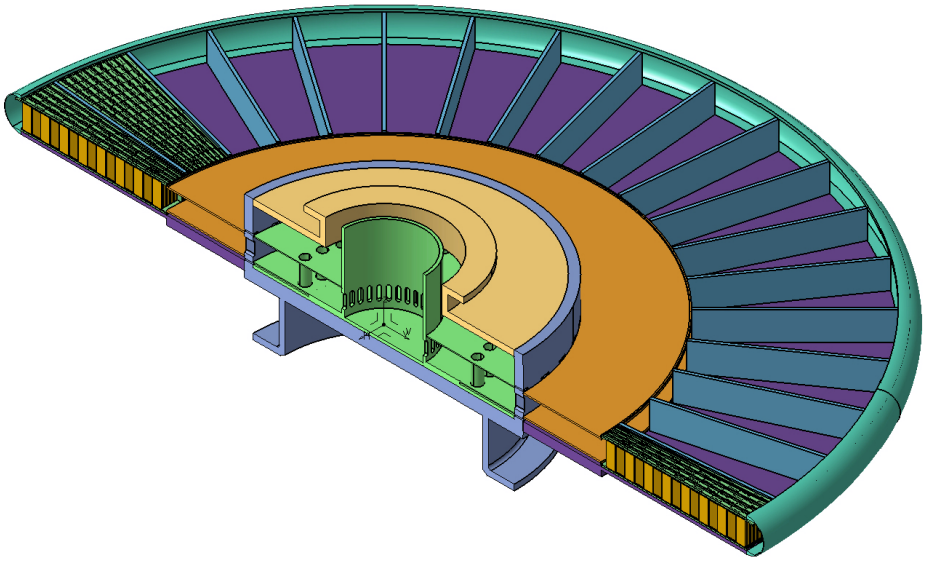

Figure 2: Target wheel configuration

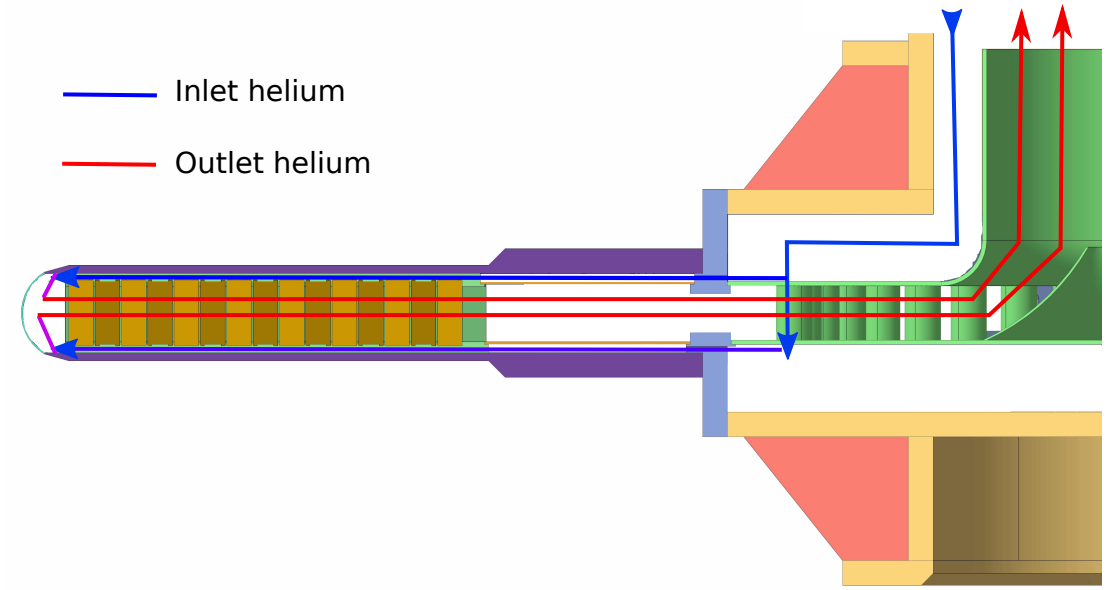

-

Figure 3: Target wheel helium flow

The coolant goes into the wheel by means of a $\sim$ 6-7 m coaxial shaft. The cold helium flows thought the external region of the coaxial shaft and the hot helium flows in the internal one. This configuration allows to minimize the thermal expansion.

Neutron shielding requirements makes shielding in the helium shaft channels mandatory. In order to minimize the effect of this shielding a complete optimization processes was carried out [5]. The final proposal includes three spiral channels shown on Figure 4 as a compromise between pressure drop and neutron shielding.

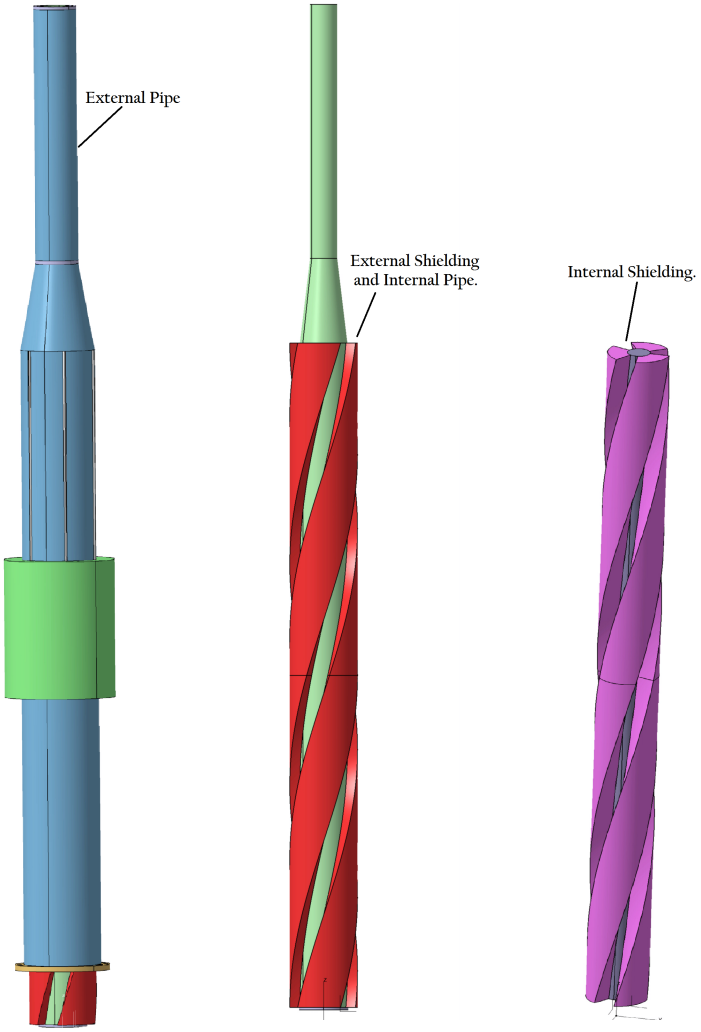

Figure 4: Target shaft w

Finally, the connection between the shaft and the main helium loop is done by means of a rotating seal. Detail analysis of this components is not in the scope of this document [6].

3 Requirements

The ESS 5 MW beam will produce a heat load in the spallation material in the range of 2.5 MW. This heat will be remove by 3 kgs^{-1} of helium at 40^oC. The main challenge of the cooling system is the relative low pressure of the loop (10 bars). This low pressure is need to avoid large thicknesses in the target steel structures that will reduce the target neutron performance.

This pressure and mass flow conditions push the helium circulator to the limit of the technology. Based on that, the total pressure drop of the target loop is one of challenges for the cooling system. On the other hand, the helium flow must to guaranty temperatures below the critical value for the spallation material.

The main requirements for the target flow path are:

- Total pressure drop of the target: Limited to 0.8 bar, being this quantity the maximum allowed in order to guarantee the pump correct functioning.[3]
- Maximum Spallation material temperature: Limited to 500^oC : so that mechanical integrity of the components does not degrade catastrophically.[4]

The spallation material arrangement has been designed based on a compromise between turbulence generation and pressure drop [7]. Also the wheel distributor was evaluated on previous analysis in order to minimize the pressure drop [5]. Following this philosophy, the connections between wheel, shaft shielding and rotating seal will be reviewed on section 5 to complete the optimization processes.

4 Methodology

The ESS Target is a complex device with 36 sub-targets (Spallation material & cassette) coupled with the coaxial shaft, the rotating seal and the central distributor . The complexity of the system and the large discrepancy between sizes of the different regions makes impossible to perform a single simulation to reproduce all the helium flow path.

As an example of the size of the model that will be needed to reproduce the complete flow path, the simplified model for one sub target has $\sim 1.4 \cdot 10^6$ elements, and the shaft region is close to $3.4 \sim 6 \cdot 10^6$. If we extrapolate these quantities, the complete model will required at least ~ 53.8 millions of elements, which make it impossible to solve without high performance computational clusters.
To address this problem, we propose to split the flow path in two regions as it is shown on Figure 5. The first sub-model reproduces the flow between the rotating seal to the internal wheel distributor. This area has large flow channels and no symmetry planes due to the helical geometry of the shaft. However, after the flow in the helix channels the helium arrives to a

region with and homogeneous pressure in from of the outlet of the central distributor.

The second sub-model includes the cassette, the spallation material and the target vessel. Due to the symmetry in the outlet of the first model, this areas shows a 1/36 symmetry thus, we only need to consider and small fraction of the geometry. However, the small size of the flow areas introduces additional complexity and requires more detailed modeling.

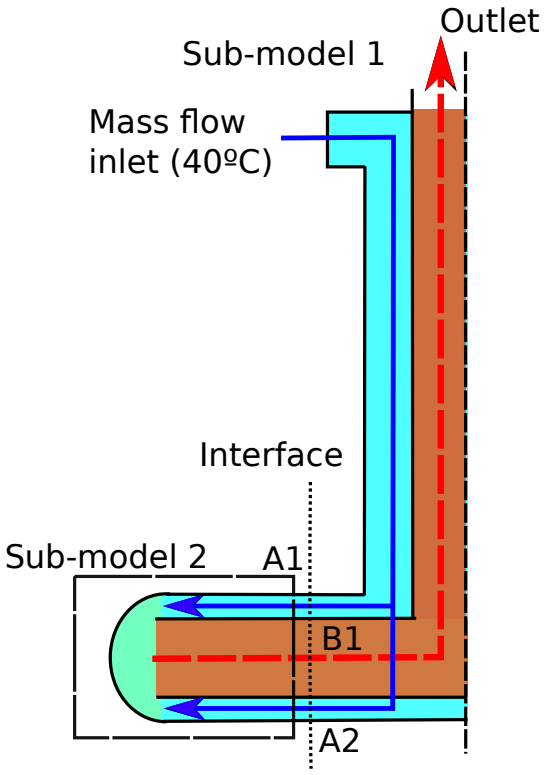

Figure 5: Sub-models description

4.1 Sub-model 1: CFD model for the distributor, shaft and rotating seal

The sub-model 1 comprehends three clearly differentiated sections that has been considered for the analysis:

Rotary Seal:

The rotating seal is in charge of connecting the inlet and outlet pipes (static elements) with the Target shaft (rotating elements). Thus, two ferrofluid seals are needed to avoid helium leaks. The analysis of this component is not in the scope of the document.

The relative movement between static and rotating areas of the component produces a transitory problem. However, the complexity and size of the geometry makes extremely difficult obtaining the solution on non stationary conditions. In order to simplify the problem, we will analyze it in steady state conditions when the relative position between seal and shaft produces the maximum pressure drop. The geometry is shown on Figure 6.

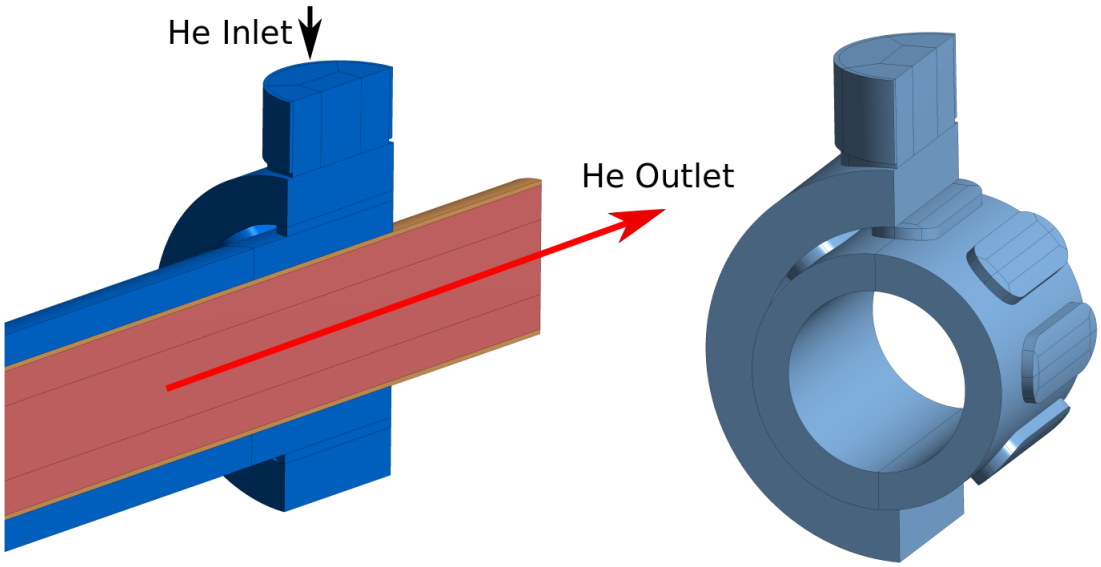

Figure 6: Rotary feedthrough cold fluid domain

Shaft:

The shaft is the element that connects the rotating seal with the Target wheel. As it was described on previous sectors it is an almost 7 m long coaxial pipe with steel shielding inside. Three helium channels for inlet and outlet are drilled in the shielding following an spiral shape. The Figure 7 shows the helium flow path. Solid elements in the shaft (shielding and internal-external pipes) have been considered to reproduce the heat flux between channels.

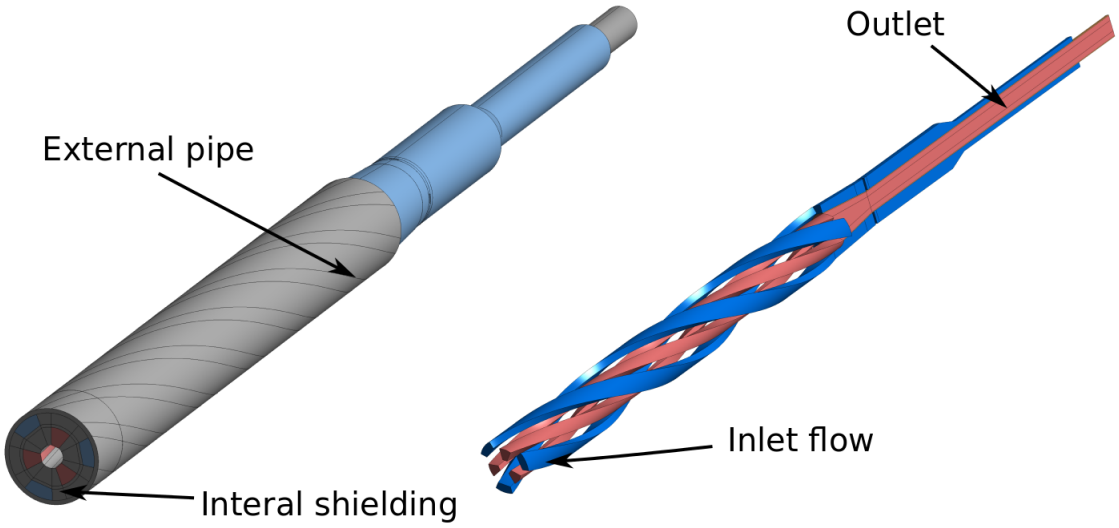

Figure 7: Shaft CFD domains

The Figure 8 shows the manufacturing test for the production of these helium channel along the shielding. The test shows that the proposed geometry is feasible in an acceptable cost and quality.

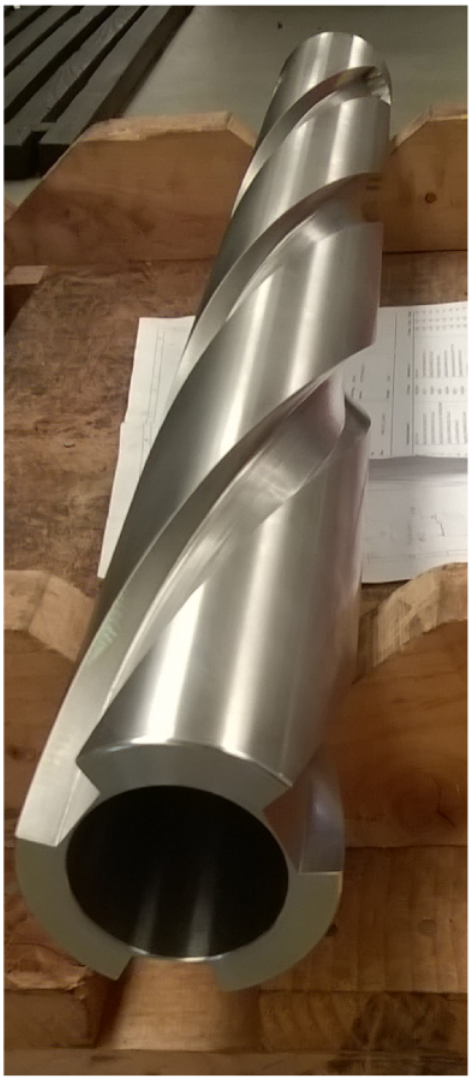

Figure 8: Helium channel manufacturing test

Distributor:

The distributor is the region of the target wheel in with the helium coming for the shaft is divided in 72 radial flows. Also the outlet flow is collected from 36 radial pipes and guide to the three spiral outlet channels.

The flow path is shown on Figure 3. The cold helium coming from the external area of the shaft is collected in a large volume in which the pressure is homogenized (volume 1) in from of

36 radial channels to the top vessel. Also, this volume is connected by means of several vertical pipes to a second volume in the lower part of the wheel. This second volume produces an homogeneous pressure in from of the 36 bottom channels. It should be remark that the pressure drop between the regions is adjusted in the "lib" of the cassette that produces a higher pressure drop in the vessel top channels to compensate the pressure drop in the connection pipes between the two distribution volumes.

Regarding the hot helium it arrives radially by means of 36 large diameter pipes. It is collected in a large central volume that homogenizes the pressure before the connection to the outlet channels.

The different flow regions considered in the simulation model are shown on Figure 9. The solid plates the separates the hot and cold flow are also considered in the model in order to reproduce the right heat exchange between the channels.

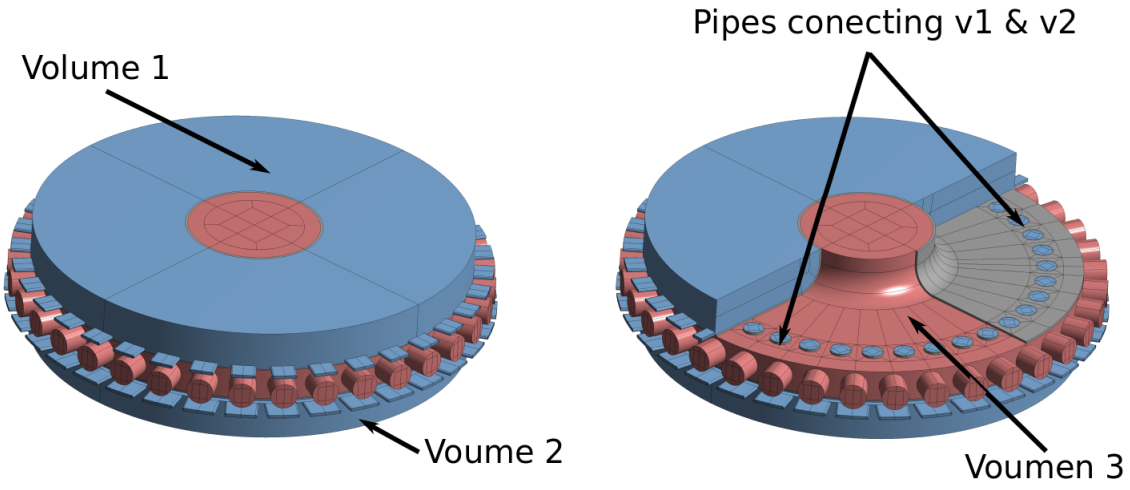

Figure 9: Distributor CFD domains

4.2 Sub-model 2: Target CRD model

The Sub-model 1 ends in the radial outlets and inlets of the distribution. This surfaces shows a symmetric distribution of the helium flow and they are connected by the Target sub-model as it is shown on Figure 5. Figure 10 shows the different element that have to be consider in this sub-model.

The detail analysis and optimization of the helium flow in spallation material was develop on previous analysis [7]. The 2 step analysis proposed can not be applied to the complete cassette region (cassette channels, proton beam entrance window, spallation material and outlet volume). Thus, in order to address the problem, a simplified model is needed.

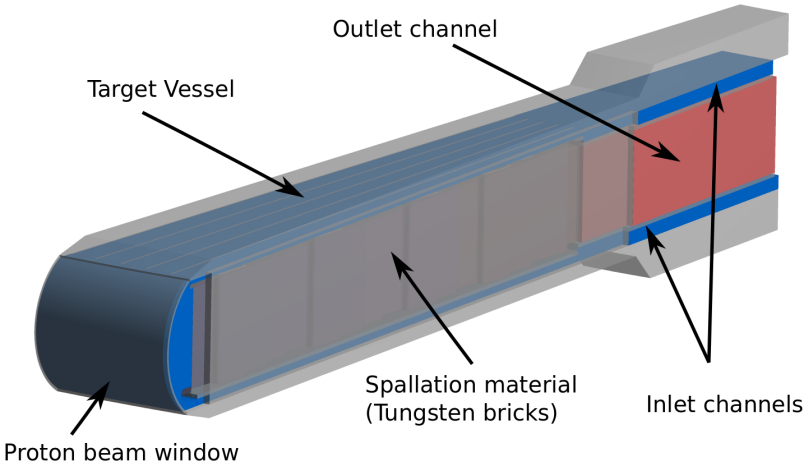

Figure 10: Target

The simplification of the model is done by removing the geometry of the cassette facing the spallation material. As it is shown on EED for cassettes[8], the spallation material is introduced in “grooves“ in the cassette. These grooves ($\sim$ 2 mm in hight) has been removed to the model. Besides that, the expansion gap in between the cassette and the spallation material has been removed. With these simplifications, the spallation material region can be meshed "sweeping" with 6 elements in the vertical direction(Figure 14). This process gives an acceptable number of elements but, we lose precision in the temperature distribution on the spallation material.

However, this simplifications change the heat flux in between spallation material and the cassette. In order to correct this effect, two thermal resistances has been introduced in between cassette and spalation material to reproduce the heat flux according to the detail cassette analysis[7]. The Figure 11 shows the positions and the values of the thermal contact resistance. Obviously the thermal resistance in the top of the cassette is higher due to the effect of the

expansion gab.

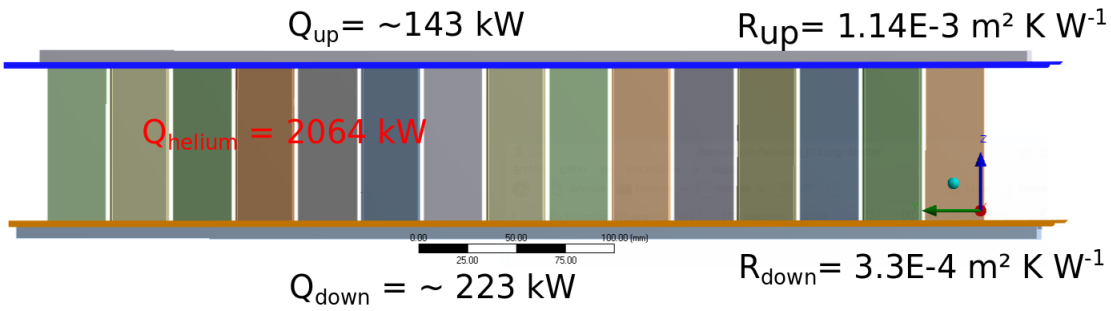

Figure 11: Target thermal resistances in the contact between cassettes and spallation material

The model reproduces the heat valance of the system with 85% removed by the helium flow in the spallation material, 9% moved to the bottom channels and 6% to the top ones.

4.3 CFD mesh

A complete structured grid (Hexas) has been created throughout the solid and fluid volumes for both sub-models. The quality analysis for both sub-models is summarized on Table4.3, in which acceptable average values is shown. By adequately distributing the grid a 3.4 million element grid was obtained for sub-model 1 and 1.4 million for sub-model 2.

	Shaft Seal+Shaft+Distributor		
	No Adapted	Adapted	Target
N^o Elements	3398894	3376444	1401759
(fluid)	3150260	3122560	1075890
(solid)	248634	253884	325869
Orthogonal Quality	0.973	0.971	0.944
Skewness	0.097	0.100	0.171
Aspect Ratio	6.805	6.953	57.96

Table 1: Mesh quality for sub-model 1 and sub-model 2

Due to the ambition of this analysis in terms of geometry and number of sections, it could have not been made without making the effort to accommodate a complete hexahedral grid to the model, otherwise the number of elements will have been considerably bigger than our computational resources could handle, and the stability/convergence of the solution even more complicated to deal with. Figure ?? and ?? shows the mesh along the shaft helical channels in which a sweeping process along the flow paths can be notice. Figure 14 shows the mesh in the critical areas of the sub-model 2.

It should be remarked that boundary layer mesh has been generated according to the Y^+ required as explained in the modeling section of the document.

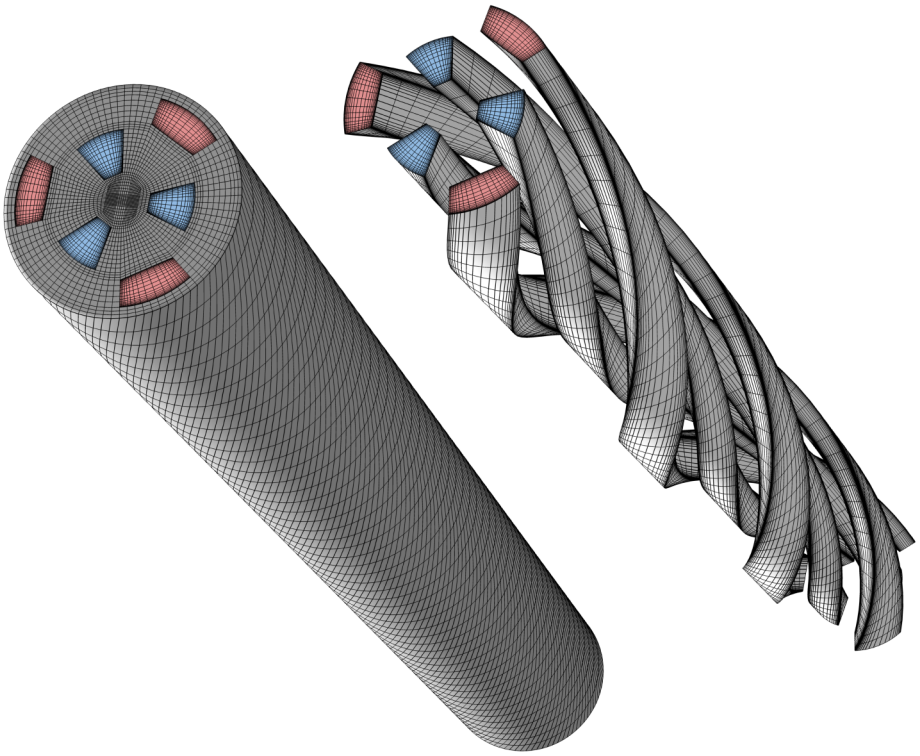

Figure 12: Shaft helical channel mesh

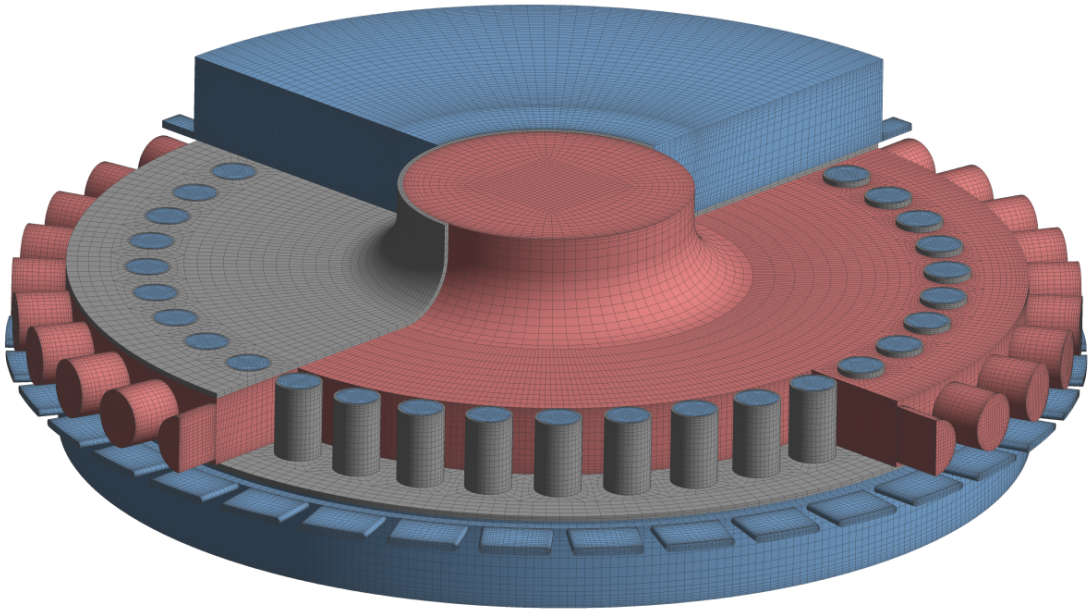

Figure 13: Central distributor mesh

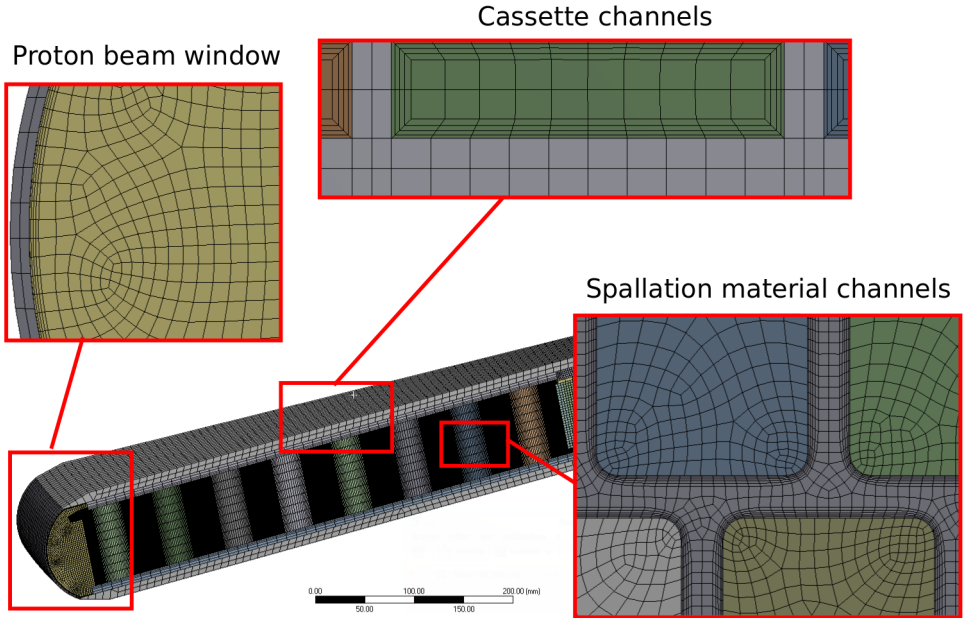

Figure 14: Target mesh

4.4 Physics Modelling

An steady state analysis with compressible pressure-based coupled solver has been executed. Pressure based solvers have been widely improved since its beginnings (when it was originally meant for solving incompressible flows) for being able to handle compressible flows such like this.

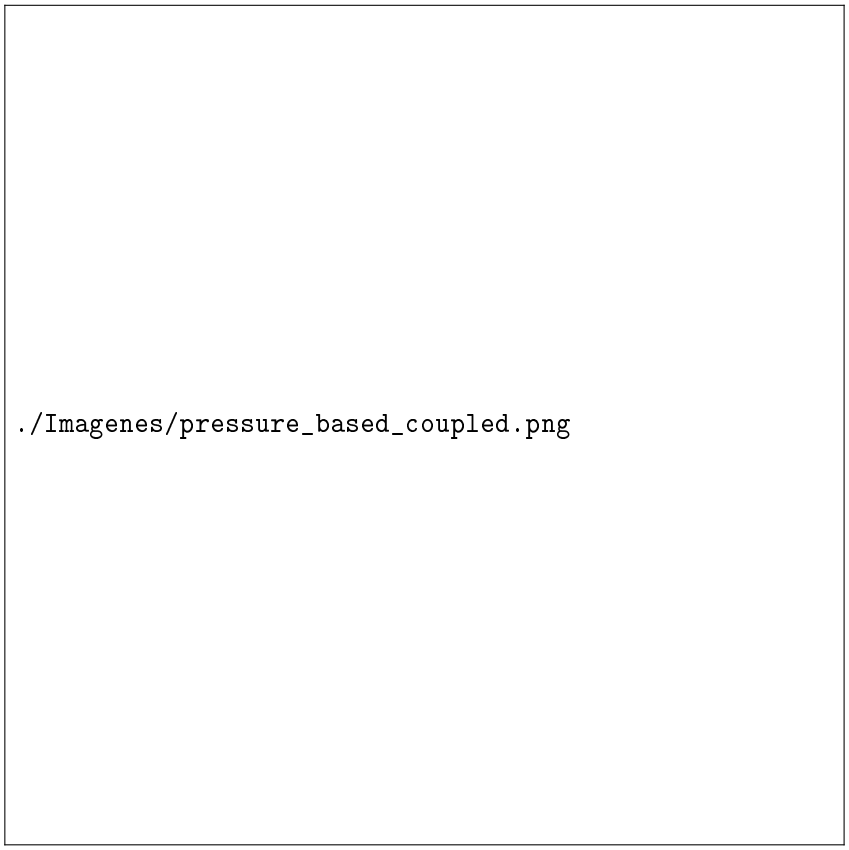

Figure 15: Overview of the Pressure-Based Coupled Algorithm

This algorithm solves a coupled system of equations for momentum and continuity in contrast to segregated methods that solve variables one after another which is obviously more memory efficient (1.5 to 2 times) but also presents slower convergence. Not being memory resources our limitation in terms of computation a coupled algorithm is the right approach.

4.4.1 Turbulence modelling

In order to solve the turbulence, $\kappa-\epsilon$ model has been used. Its efficacy in full turbulent developed flows while been computationally cheap have made it widely used in pipe flows similar to the one seen in the seal, shaft and distributor components. For the target sector flow has been also initially solved with this method for stability purposes, however do to the narrow dimensions of the channels the coolant flows trough this method solution was used as the initial departure

point for a $k-\omega$ turbulence model analysis that better solves regions near walls, critical for accurately solve this section of the loop.

4.4.2 Wall approach

For solving the near wall region at the seal, shaft and distributor sectors a Standard Wall Function model is implemented so the first cells height from the wall is such that the Y^+ belongs to the interval (30-300) valid for this method.
However in the target flow near walls has been entirely solved up to the wall so $Y^+ \approx 1$ is needed.

5 Optimization process

As it was remarked on Section 3 the initial shaft configuration shows a hight pressure drop, mainly due to several transitions areas. Taking into account that pressure drop is one of the critical requirements for the target, new elements and modifications in the initial geometry has been made in order to diminish it.

Considering that the complete mesh model has around five million elements, the CFD studies of the changes has been limited to the region in which the modification has been made. Obviously every element modified or introduced will change flow characteristics throughout all the domain, however pressure drop reduction can be greatly appreciated if we limit our study to the most affected section of the loop.

For three out of the four sections mentioned on the model description (section 4.1), the optimization has been completed. On Section 6 the complete model has been evaluated with and without this optimization process in order to confirm the methodology of partial modeling proposed on the optimization process.

5.1 Rotary feedthrough

The most evident drop in pressure comes from the fluid trying to pass through the holes that communicate the rotating components with the static ones.

In order to reduce this drop it seems logical that this holes should be made as large as possible. It can also be appreciated that the flow entering the holes is not the same for all of them, so by increasing the volume of the outer ring that the holes communicates with upstream, there will be more room for accommodating the fluid to this geometry (Figure 16).

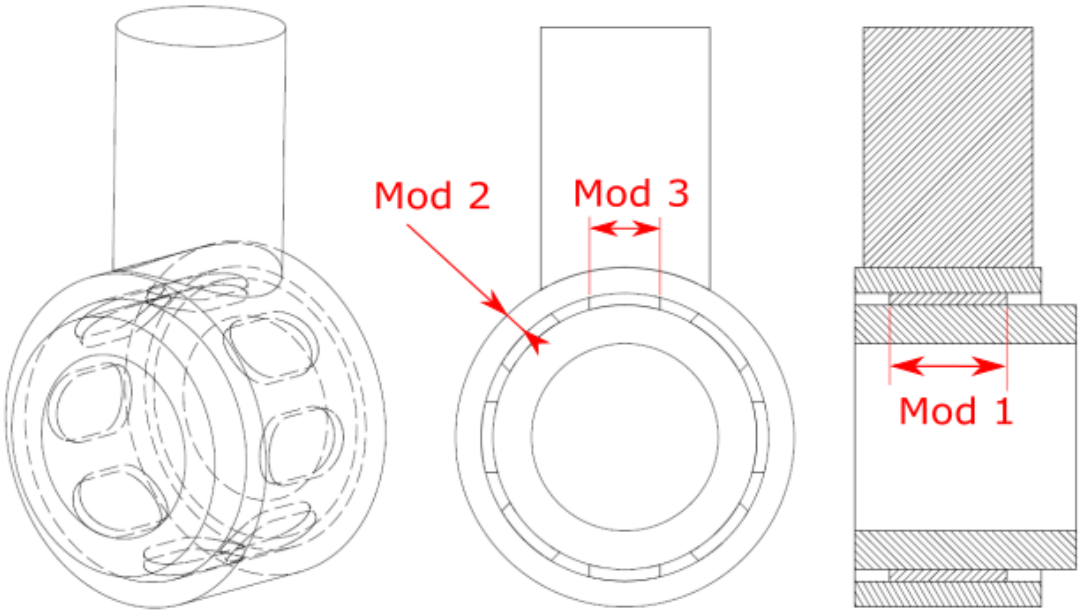

Figure 16: Rotary feedthrough modifications

5.1.1 Modification 1

In order to increment the size of the holes the first dimension that can be modified is their length which has no other the limit than the solids around so the maximum value possible has been chosen. Table 2 shows the pressure drop reduction by increasing the inlet diameter. There is a considerable reduction in terms of pressure drop which justifies the change.

Diameter (cm)	Pressure Drop (Pa)
10	29801
16	15543

Table 2: Pressure drop change with width.

5.1.2 Modification 2

The inlet helium is distributed on a ring in order to distribute the flow along the shaft diameter. The increase of this thickness increase the fraction of the helium that moves into the shaft by connections not in from of the inlet pipe. Table 3 shows the evolution of the pressure drop increasing the dimensions of the connection ring.

Hight (cm)	Pressure Drop (Pa)
2.2	15543
3.0	13254
5.0	12151
6.5	11848
8.0	11926

Table 3: Pressure drop change with width.

If the diameter grows over 0.05 m there is now significant decrease in pressure lost to justify the change so this is the value given to the outer diameter.

5.1.3 Modification 3

Attempting to reduce even more the pressure drop the width of the shaft openings has been increased up to a limit were the structural integrity of the tube region in between the holes can be guaranteed. Table 4 shows the evolution of the pressure drop. The Table shows that if we make the holes as wide as possible we will reduce the pressure drop even more however this will made the region between the holes extremely narrow and structurally weak, thus considering the reduction in terms of pressure drop is not that high the wide chosen for the design will be 3 cm.

Width	Pressure Drop
(cm)	(Pa)
3.0	12153
3.25	11959
3.50	11477
3.75	10933
4.0	10267

Table 4: Pressure drop change with width.

5.1.4 Feedthrough modifications summary

Considering the three modifications, the pressure drop in this section can be reduced from 29801 Pa to 12153 Pa which makes a big difference if we consider that the maximum drop allowed all over the loop is 80000 Pa. Figures 17 and 18 shows pressure and velocity for the the sequence of modifications.

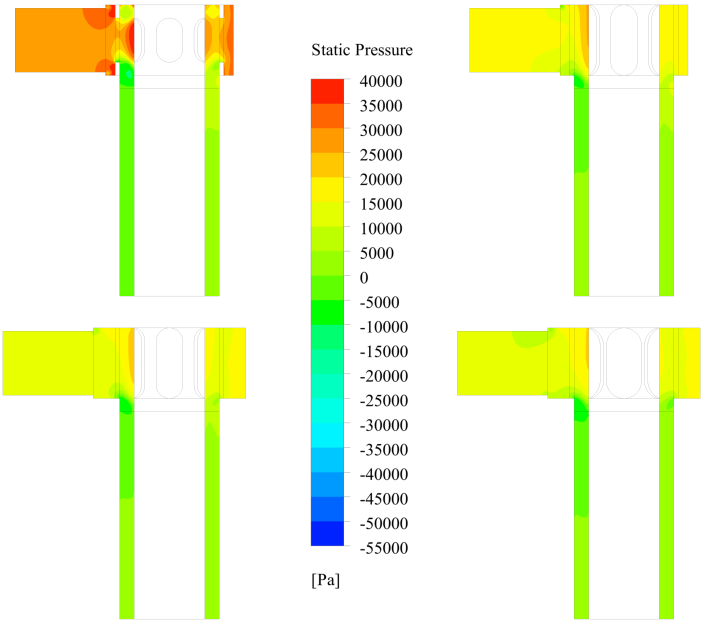

Figure 17: Pressure distribution at rotatory feedthrough symmetry plane. Top left: Original design. Top right: Modification 1. Bottom left: Modification 2. Bottom right: Modification 3

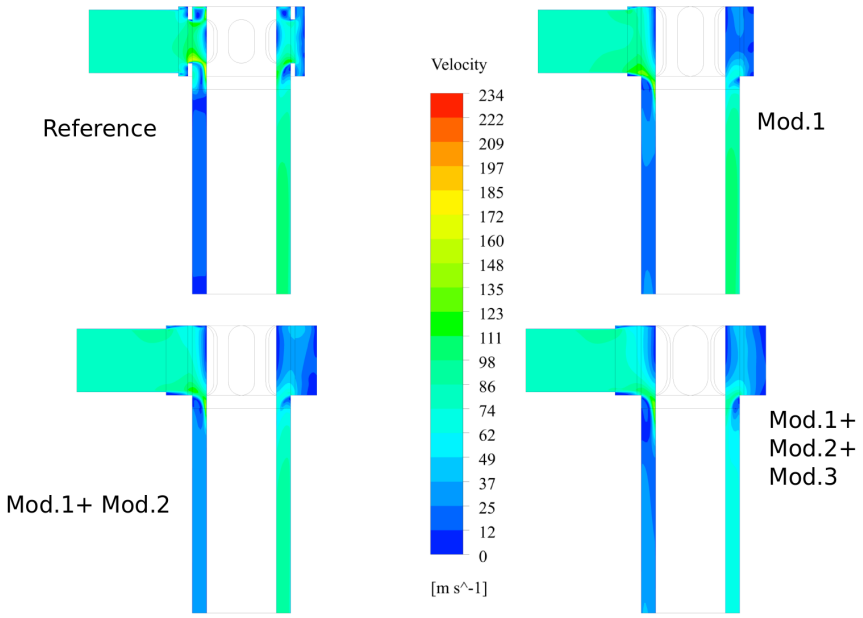

Figure 18: velocity distribution at rotatory feedthrough symmetry plane. Top left: Original design. Top right: Modification 1. Bottom left: Modification 2. Bottom right: Modification 3

5.2 Shaft inlet

The connection between the open volume on top of the shaft and the eliptical channels is one of the main sources of pressure drop due to the large change in the flow section.

In order to improve this transition, three identical pieces have been introduce to smoothly adapt the flow to the three channels of the helix. Figure 19 shows the additional elements added to the shaft geometry.

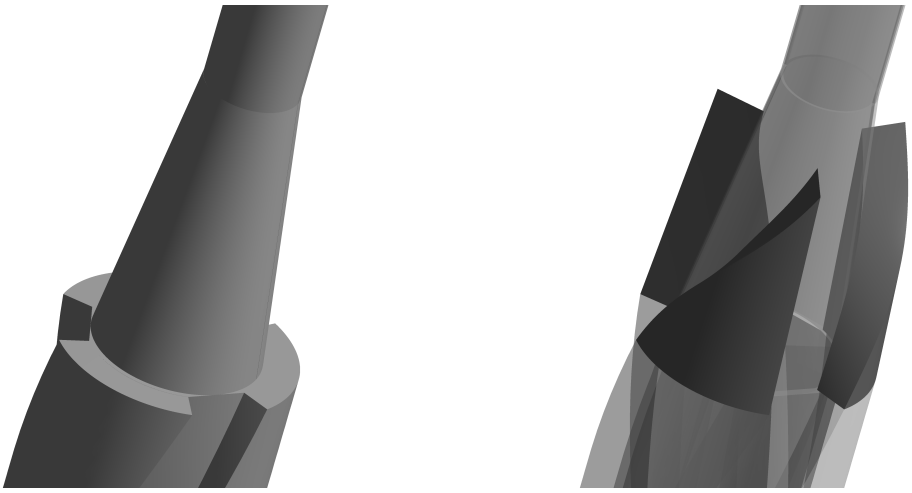

Figure 19: Shaft modifications

Table 5 shows the reduction in the pressure drop due to the introduction of this transition elements. Despite of the fact that the transition elements increase the complexity of the manufacturing the reduction of the pressure drop clearly justifies the modification.

Geometry	Pressure Drop
Original	14415
Modified	10300

Table 5: Pressure drop change with additional pieces.

Figures 20 and 21 shows the pressure and velocity profiles after and before the modification. The original geometry produces a clear boundary layer detachment that reduces the effective size of the cross section to half. The new geometry correct this effect and produces a smooth evolution of pressure and velocity with laminar flow.

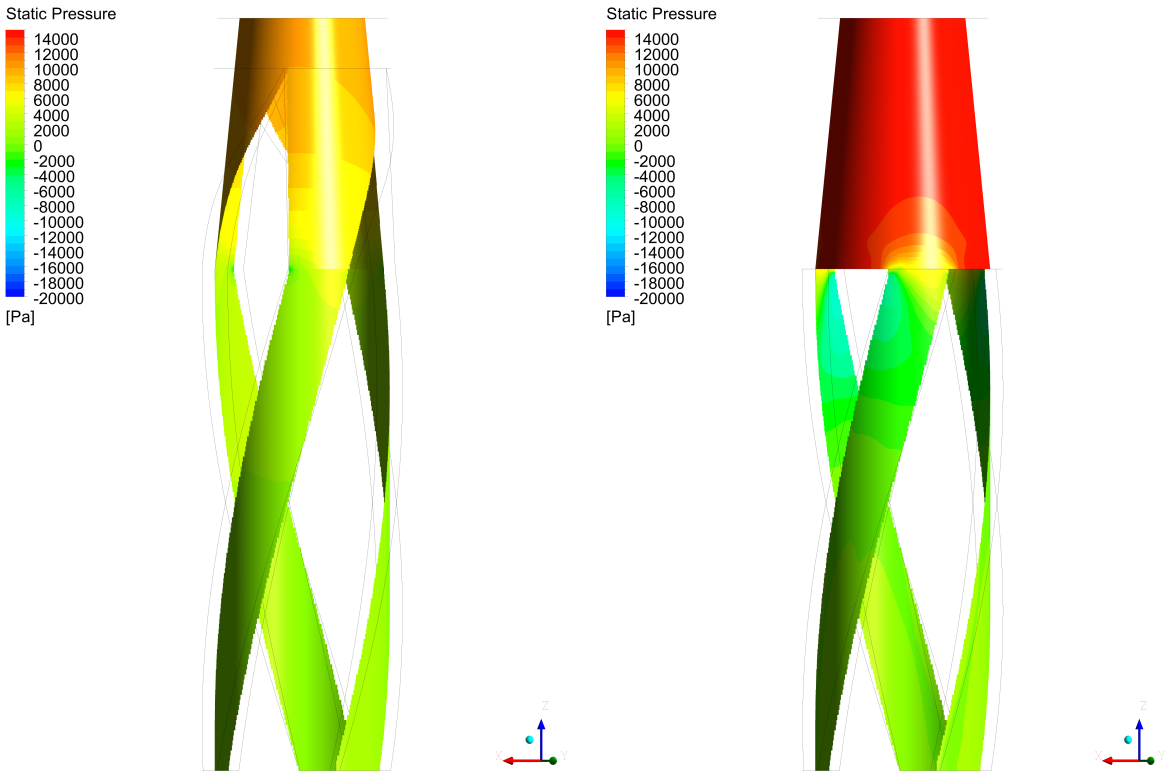

Figure 20: Pressure distribution at rotatory shaft shielding inlet. Left: Original design. Right: Modification

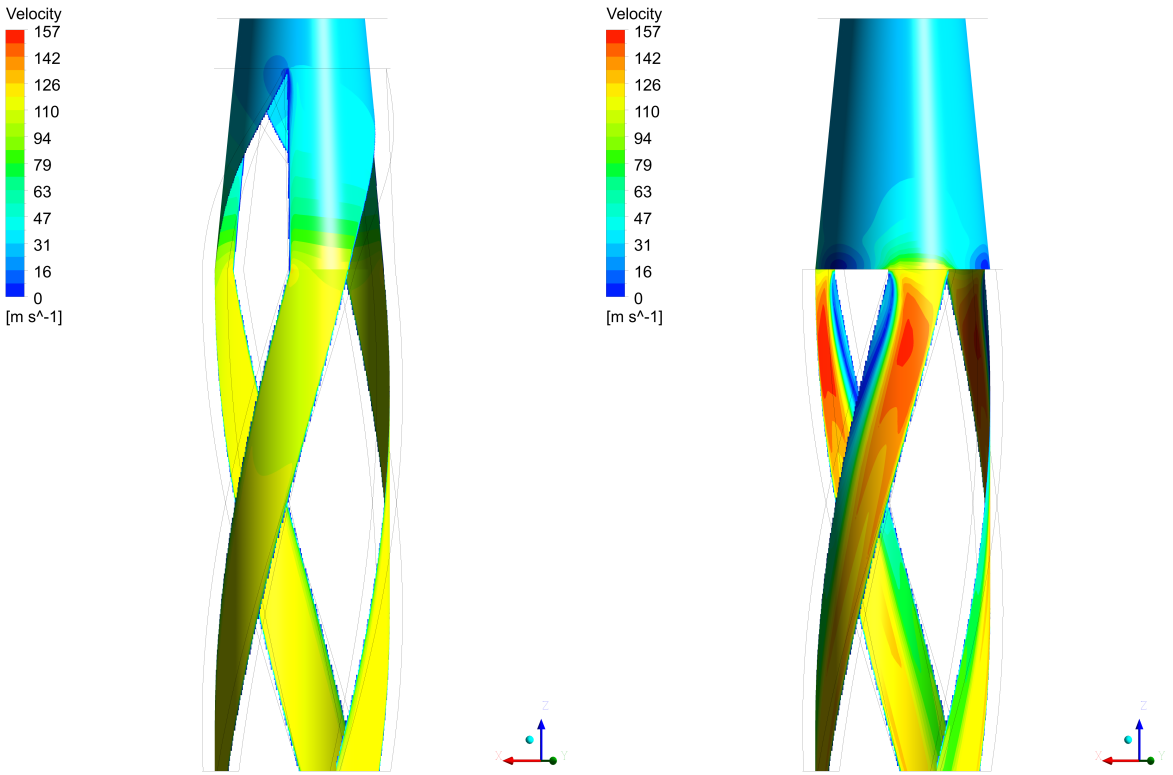

Figure 21: Velocity didistribution at rotatory shaft shielding inlet. Left: Original design. Right: Modification

5.3 Outlet distributor

The central distributor for the outlet flow channel the 36 radial collectors to the three spiral channels on the inner shielding. Form the fluid dynamic point of view, the problem is similar Shat inlet (See section 5.2): a flow at low hight pressure and low velocity force to move in smaller cross section. This configuration process a high pressure drop, even more in this case due to the higher temperature of the outlet flow.

To reduce the pressure drop, several elements with convergence thickness has been introduced in the model in order to channel the flow. In order to simplify the analysis, the distributor has been simulated with 1/3 symmetry. The new elements introduced in the flow can be shown on Figure 22.

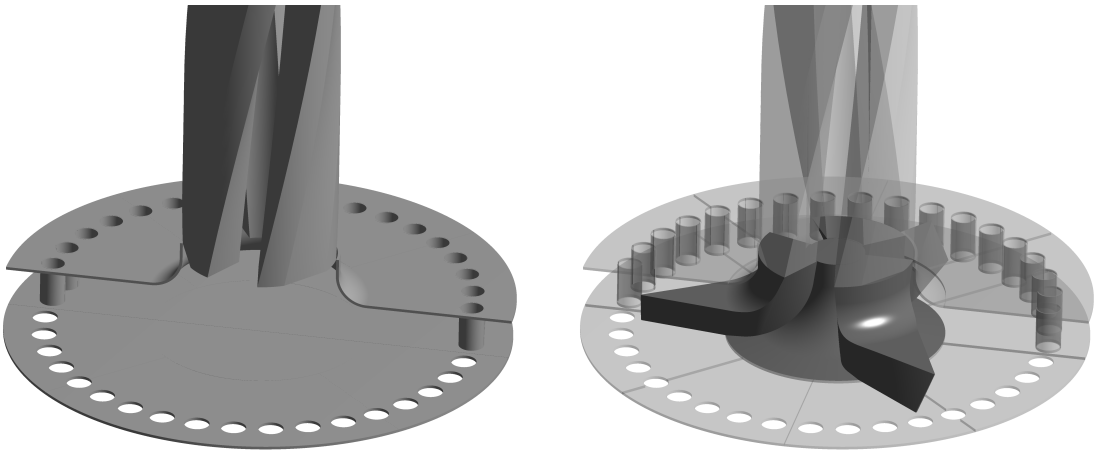

Figure 22: Shaft modifications

Table 6 shows the total value for pressure drop for nominal an upgrades design. In this case, the increase of complexity on the manufacturing will be significant but it is justify but the pressure drop results. Figure 23 shows the pressure distribution for both cases.

Geometry	Pressure Drop
Original	26117
Modified	19092

Table 6: Pressure drop change with additional pieces.

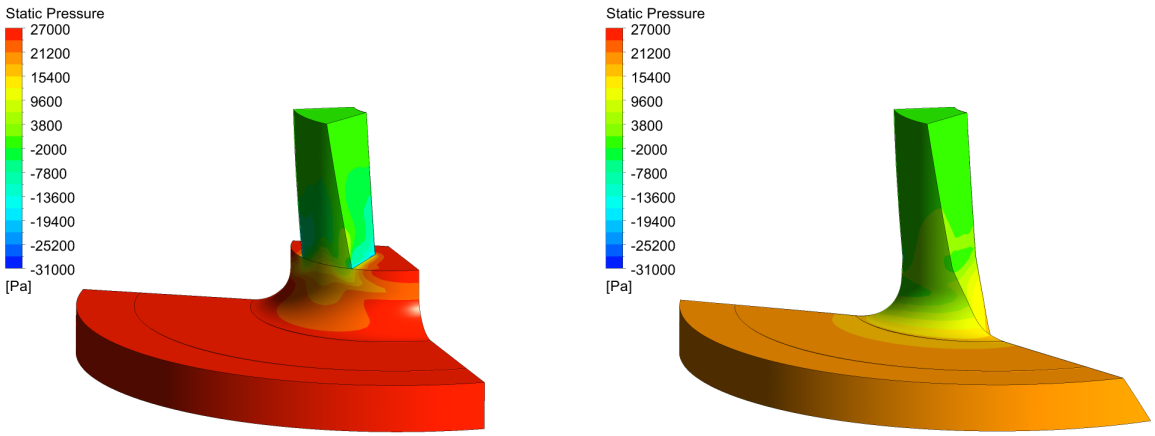

Figure 23: Pressure distribution at distributor sector. Left: Original design. Right: Modification

6 CFD complete analysis

This section shows the complete results of the CFD study considering all the elements mentioned above in this text. Following the methodology described on Section 4, the Target is divided in two sub-models: sub-model 1 (Figure 24) and sub-model 2 (Figure 25). Boundary conditions are coupled so, iterative resolution is needed to find the right boundary conditions for both models.

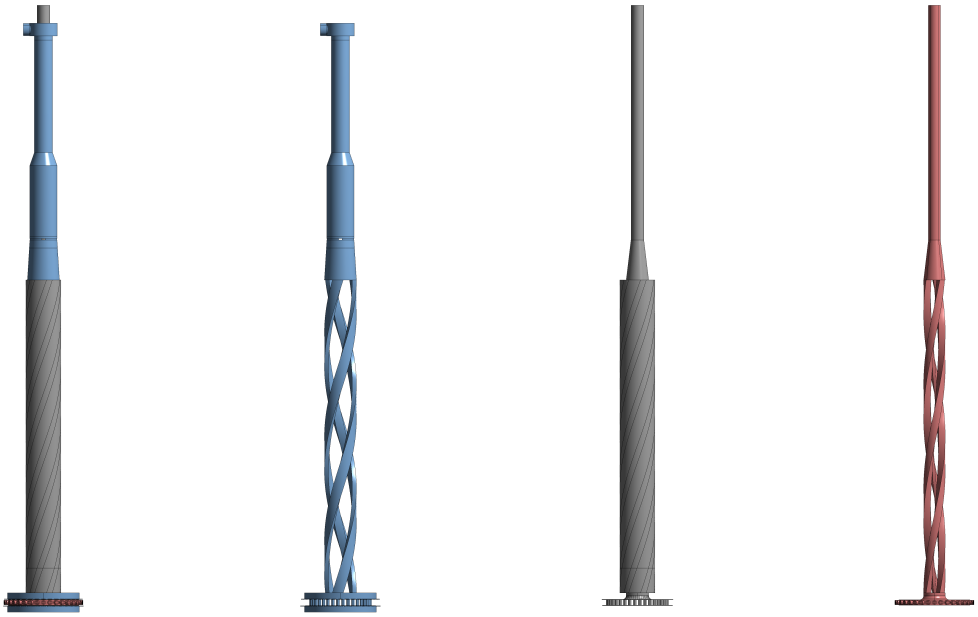

Figure 24: From left to right: Studied components of the loop from the rotary feedthrough to the distributor, cold fluid, solids and hot fluid from this same section. Three material zones are easily distinguished: Cold fluid (blue), hot fluid (red) and solid (gray)

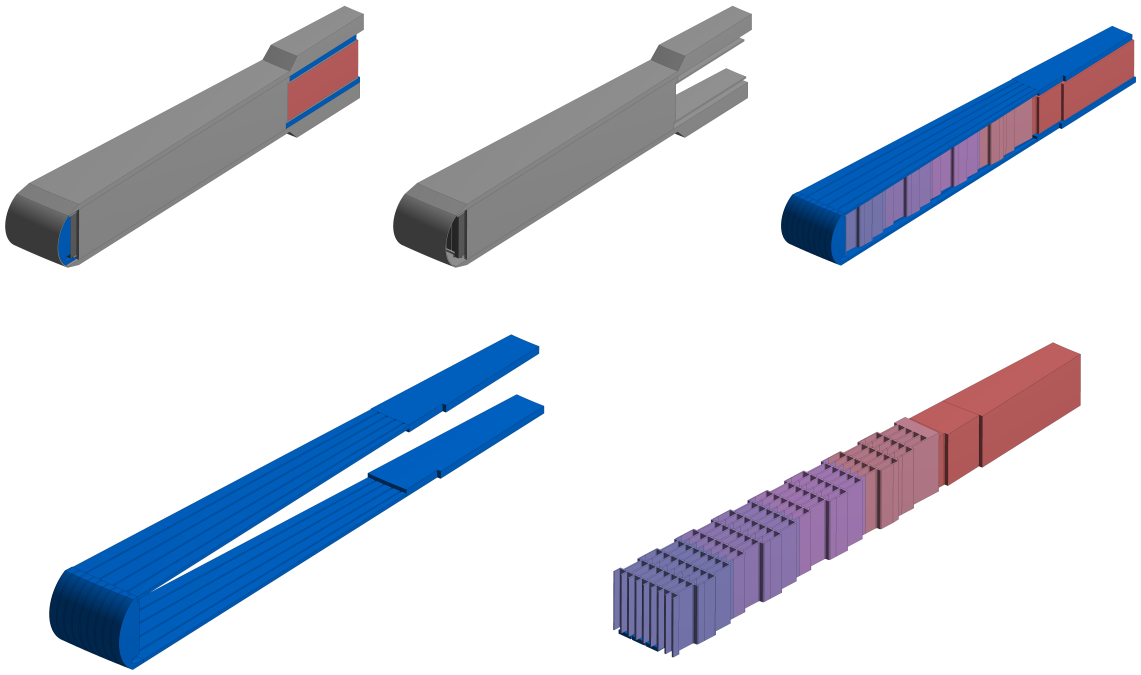

Figure 25: Target representation of solids and fluid being heated while going through the bricks.

The optimization process described on Section 5 proposes several modifications in the reference geometry to reduce the pressure drop. Modifications associated to the feedthrough do not show any clear drawback to, it will be implement. However, the introduction of the transition elements in the shaft geometry will force us to a more complex manufacturing process. In order to confirm previous analysis the reference geometry and the updated configuration (including transition regions) has been evaluated.

Trying to anticipate a possible reduction of the mass flow through the loop imposed by the pressure drop limitation, the analysis has been made for a range that goes from a 15% reduction of the initial considered mass flow (3kg/s) up to the 100% in 5% leaps. Tables 7 and 8 shows the temperature and pressure drop evolution for reference and updated geometries.

The maximum temperature of the bricks as well as every other temperature value showed does not seem any change due to the introduction of the transition regions. Regarding the pressure drop, it reflects a reduction of $\sim$ 0.1 bar with the introduction of this elements so, the modification is recommended even if it introduces a more complex manufacturing process. However, the total pressure drop at nominal mass flow is still above the requirement.

Tables shows the evolution of maximum temperature in the spallation material and pressure drop when we reduce the mass flow. It can be remarked that an lightly reduction of the mass flow wll reduce the pressure drop up to acceptable levels without producing temperatures in the spallation material above the design criteria.

	OULET TEMPERATURES (^oC)									
	Reference					Updated				
MF(kg/s)	A1	A2	B1	B2	W_{max}	A1	A2	B1	B2	W_{max}
3.00	56	63	183	206	373	57	63	182	206	373
2.85	57	65	192	217	390	59	66	191	217	390
2.70	59	66	200	226	411	60	68	199	226	411
2.55	61	69	210	238	433	62	70	209	238	433

Table 7: Temperature on interface between sub-models (Figure 5) and maximum time averaged temperature in the spallation material

	PRESSURE DROP (Pa)							
	Reference				Updated			
MF(kg/s)	Cold	Target	Hot	TOTAL	Cold	Target	Hot	TOTAL
3.00	38277	16300	43260	97837	34834	16300	37594	88728
2.85	34761	15300	40022	90083	31733	15300	34793	81826
2.70	31429	14200	36663	82292	28801	14200	31881	74882
2.55	28223	13300	33566	75089	25662	13300	29181	68143

Table 8: Total pressure drop for sub-models (Figure 5)

7 Conclusion

As main conclusions of the analysis several points can be remarked:

- A complete CFD analysis considering all the elements of the ESS Target has been completed.
- The optimization process of the transient sections between elements has been completed. The modifications proposed reduces significantly the total pressure drop.
- Despite of the modification process, it will be really complex to achieve pressure drop values below 0.8 bar nominal mass flow conditions.
- However, it the mass flow is reduced from 3.0 to 2.7 $kg \cdot s^{-1}$, we will fulfill the requirements on maximum temperature in the spallation material ($411^oC < 500^oC$) and total pressure drop ($0.75 < 0.8$ bar).

References

[1] Reference is needed.

[2] ESS-0036673: ESS-Bilbao Target Proposal

[3] ESS-0019346: ICP PCool Target

[4] ESS-0003310: Beam on Target Requirements

[5] ESS-0040121: Target shaft design

[6] ESS-0066410: Mechanical Analysis of the Shaft following RCC-MR$_x$ N2$_{Rx}$

[7] ESS-0058358: EQUIPMENT SPECIFICATION DOCUMENT: SPALLATION MATERIAL

[8] ESS-0059935: Equipment specification document: Internal structures - cassettes